analytical chemistry

Article

Cite This: Anal. Chem. 2019, 91, 15899−15907

pubs.acs.org/ac

Organelle-Redirected Chameleon Sensor-Enabled Live Cell Imaging of Mitochondrial DNA

Xiaoxue Zou,[†,§] Yilong Shi,[‡,§] Rui Zhu,[†] Jiahuai Han,[‡] and Shoufa Han*[,†,‡]

[†]Department of Chemical Biology, College of Chemistry and Chemical Engineering, State Key Laboratory for Physical Chemistry of Solid Surfaces, the Key Laboratory for Chemical Biology of Fujian Province, the MOE Key Laboratory of Spectrochemical Analysis & Instrumentation, and Innovation Center for Cell Signaling Network, Xiamen University, Xiamen 361005, China

[‡]State key Laboratory of Cellular Stress Biology, Innovation Center for Cell Signaling Network, School of Life Sciences, Xiamen University, Xiamen 361005, China

Supporting Information

ABSTRACT: Mitochondrial DNA (mtDNA) plays important roles in diverse physiological processes and myriad diseases. We herein report mtDNA imaging with a chameleon sensor containing a cationic rhodamine B (RB) entity for mitochondria targeting and a fluorogenic SYBR Green-I (SG) entity for DNA sensing. SG-RB selectively binds to mtDNA and gives green SG fluorescence in mitochondria of living cells but gives red RB fluorescence upon delivery of mitochondria into lysosomes in mitophagy. With the dual-color imaging, mtDNA aggregation and elevated mitophagy were identified in HeLa cells stressed with anticancer doxorubicin. These results suggest the utility of organelle-redirected DNA sensors for live cell imaging of mtDNA involved in myriad pathological disorders.

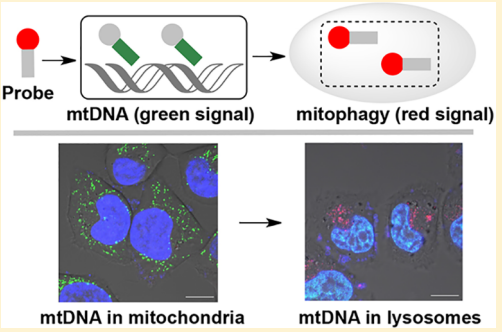

Mitochondria are ubiquitous mammalian organelles critical for diverse cell activities ranging from ATP production to cell death.[1−3] As the endosymbiont evolved from ancient proteobacterium, mitochondria contain inflammatogenic circular DNA with similarities to bacterial DNA.[4,5] Encoding proteins requisite for oxidative phosphorylation, mtDNA is essential for bioenergetics of eukaryotic cells. On the other hand, mtDNA is the causal agent of several inherited diseases and is also a major type of danger-associated molecular pattern engaged in inflammation, autoimmunity, and aging.[6−11] As such, techniques allowing live cell imaging of mtDNA are of significance in cell biology and biomedical research.[12−15] Although fluorogenic DNA intercalators have been widely employed in industry and cell biology, as evidenced by the use of SYBR Green-I in PCR and Hoechst in nucleus staining, direct application of these probes to live cell imaging of mtDNA is often hampered by their intrinsic affinity to nuclear DNA (nuDNA).[16]

Mitochondria are hallmarked with negative transmembrane potentials ($\Delta\Psi$m) essential to mitochondrial functions.[1−3] Cationic dyes, such as rhodamine 123, effectively accumulate in mitochondria driven by $\Delta\Psi$m.[17] In principle, partitioning of fluorogenic DNA probes in mitochondria could minimize interference of nuDNA and allow in situ mtDNA binding which gives "turn-on" fluorescence. Given the paucity of imaging agents for mtDNA[12−15] and the use of cationic species to deliver chemodosimeters or therapeutics into mitochondria,[18−25] we envisioned that integration of a mitochondria-trappable entity with a fluorogenic DNA intercalator might afford an alternative approach suitable for live cell mtDNA imaging. Hence, we synthesized SG-RB featuring a cationic rhodamine B entity for mitochondria targeting and an entity of SYBR Green-I (SG), a commercial profluorophore known to give green fluorescence upon binding to double-strand DNA (Scheme 1).[26,27] As expected, SG-RB selectively stains mtDNA, giving rise to green SG fluorescence in live cells. Moreover, SG-RB/mtDNA complex exhibited restored red rhodamine fluorescence and a loss of green SG fluorescence upon delivery of mitochondria into lysosomes in mitophagy. These attributes enable dual-color imaging of mtDNA in cells dosed with anticancer drug doxorubicin.

EXPERIMENTAL PROCEDURE

Materials and Methods. LysoTrackers, Hoechst, and MitoTrackers were obtained from Thermo Fisher. RB-CAP was synthesized following a published procedure.[56] SYBR Green-I and all other dyes were purchased from Bioluminor, Xiamen. All other chemicals were purchased from Sigma unless specified. PET22b(+) vector was obtained from Addgene, isolated from Novablue competent cells, and then purified using a reported procedure.[57] The mammalian cell lines were obtained from American Type Culture Collection (ATCC) and maintained in Dulbecco's modified Eagle's medium (DMEM) supplemented with 10% fetal bovine serum, 2 mM L-glutamine, 100 IU penicillin, and 100 mg/mL streptomycin at 37 °C in a humidified incubator under 5% CO_2.

The fluorescence spectra were performed on a SpectraMax M5 instrument. Confocal fluorescence microscopic imaging was

Received: September 25, 2019
Accepted: November 19, 2019
Published: November 19, 2019

DOI: 10.1021/acs.analchem.9b04364
Anal. Chem. 2019, 91, 15899−15907

Scheme 1. (A) Schematic for Dual-Color Imaging of mtDNA with an Organelle-Trappable Fluorogenic DNA Intercalator (SG-RB) and (B) Proposed Fluorescence Response of SG-RB toward mtDNA[a]

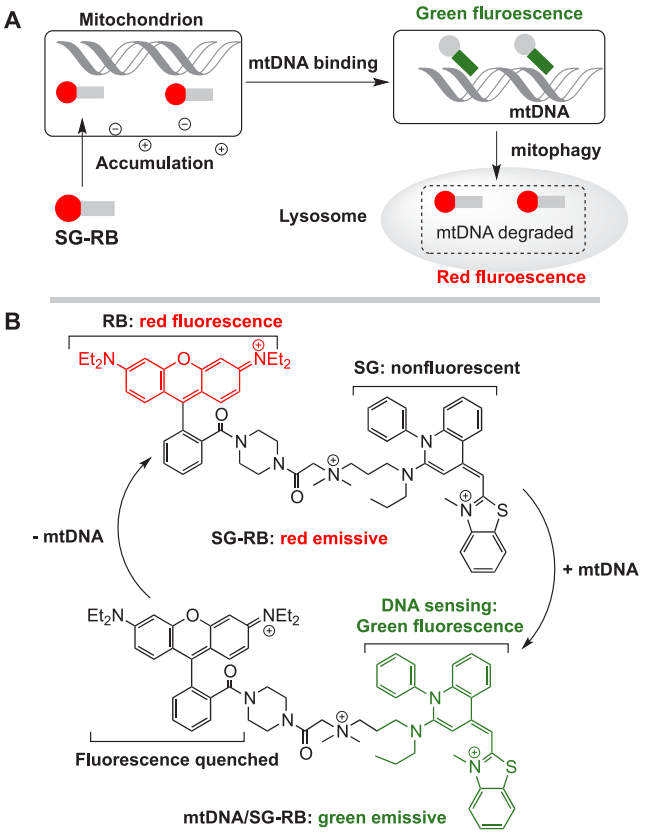

[a]SG-RB contains a cationic red-emissive RB domain for targeting mitochondria and a SG domain for fluorogenic mtDNA binding/sensing.

performed on a Zeiss LSM 780 apparatus using the following filters: λ_{ex} = 633 nm/λ_{em} = 640−680 nm for MitoTracker Deep Red, λ_{ex} = 488 nm/λ_{em} = 499−553 nm for SYBR Green-I, λ_{ex} = 561 nm/λ_{em} = 570−625 nm for rhodamine, and λ_{ex} = 405 nm/λ_{em} = 410−590 nm for Lyso-Tracker Blue. Images of merged fluorescence were processed using Zen 2.3.0. Graphs were generated by GraphPad Prism7 and origin 8.0 software.

Synthesis of SG-RB. To a flask containing *N*,*N*-dimethylformamide (DMF, 4 mL) was added SYBR Green-I (200 mg, 0.40 mmol), RB-CAP (308 mg, 0.52 mmol), potassium carbonate (K_2CO_3, 168 mg, 1.22 mmol), and sodium iodide (NaI, 300 mg, 2.01 mmol). The mixture was stirred at 60 °C overnight, and then concentrated in vacuo. The residue was subjected to silica gel chromatography (CH_2Cl_2/MeOH: 75/1) to yield SG-RB (350 mg, 82%) (Scheme 2). ^{1}H NMR (500 MHz, chloroform-*d*) δ 8.40−8.32 (m, 1H), 8.20 (d, *J* = 7.9 Hz, 1H), 7.77 (t, *J* = 7.8 Hz, 2H), 7.61 (t, *J* = 7.0 Hz, 5H), 7.55−7.50 (m, 1H), 7.50−7.38 (m, 3H), 7.36 (d, *J* = 8.3 Hz, 1H), 7.25−7.11 (m, 6H), 7.10−7.02 (m, 1H), 6.65 (s, 2H), 6.55 (s, 1H), 5.50 (s, 2H), 4.04 (t, *J* = 8.0 Hz, 2H), 3.90 (s, 3H), 3.85−3.59 (m, 8H), 3.51 (s, 6H), 3.36 (dd, *J* = 19.8, 11.3 Hz, 8H), 3.09 (q, *J* = 7.3 Hz, 2H), 1.46 (q, *J* = 7.4 Hz, 2H), 1.37 (t, *J* = 7.3 Hz, 2H), 1.27 (t, *J* = 7.1 Hz, 12H), 0.83 (t, *J* = 7.4 Hz, 3H). ^{13}C NMR (126 MHz, DMSO-d_6) δ 166.76, 162.92, 162.27, 159.18, 157.89, 157.15, 155.21, 149.11, 143.07 (d, *J* = 166.7 Hz), 140.83, 140.42, 138.67, 134.99, 132.75, 131.83, 131.01, 130.71, 130.10, 129.62, 128.23, 125.75, 125.33, 124.18, 123.6, 121.81, 118.76, 113.15, 112.73, 102.60, 96.02, 87.36, 55.09, 55.09, 51.71, 45.59, 34.00, 19.94, 12.62, 11.27. MS (ES+) calcd for $C_{66}H_{77}N_8O_3S^{3+}$ (M^{3+}) *m*/*z* = 1061.5823/3 = 353.8608. Found: 353.8612.

Synthesis of SG-C_6-RB. Rhodamine-PZ was synthesized according to the literature.[56] Rhodamine-PZ (3.4 g, 6.65 mmol) and *N*-Boc-6-aminohexanoic acid (1.69 g, 7.31 mmol) were dissolved in CH_2Cl_2 (50 mL) containing 1-(3-(dimethylamino)propyl)-3-ethylcarbodiimide hydrochloride (EDC, 1.9 g, 9.98 mmol) and pyridine (1.6 g, 20.00 mmol). The reaction mixture was stirred for 8 h and then concentrated by rotary evaporation (Scheme 3). The residue was subjected to silica gel chromatography using CH_2Cl_2/MeOH: 50/1 as the eluent to give compound **1** in 87% yield. ^{1}H NMR (500 MHz, Chloroform-*d*) δ 7.60 (d, *J* = 7.3 Hz, 2H), 7.46 (d, *J* = 7.0 Hz, 1H), 7.28−7.09 (m, 3H), 7.03−6.89 (m, 1H), 6.85−6.59 (m, 3H), 3.83 (s, 2H), 3.60−3.45 (m, *J* = 7.4 Hz, 8H), 3.32 (d, *J* = 17.7 Hz, 8H), 2.98 (q, *J* = 6.8 Hz, 2H), 2.31−2.15 (m, 3H), 1.49 (p, *J* = 7.7 Hz, 2H), 1.39 (q, *J* = 7.3 Hz, 2H), 1.32 (s, 9H), 1.23 (t, *J* = 7.2 Hz, 12H). ^{13}C NMR (126 MHz, $CDCl_3$) δ 167.30, 160.69, 160.43, 157.36, 155.80, 155.30, 134.63, 131.79, 129.85, 127.25, 120.59, 120.55, 118.23, 115.87, 114.04, 96.15, 95.79, 78.40, 49.74, 47.48, 39.89, 32.56, 29.30, 28.06, 25.98, 24.28, 9.91.

Compound **1** (1.1 g, 1.52 mmol) and trifluoroacetic acid (TFA, 4 mL) were maintained in dichloromethane (CH_2Cl_2, 12 mL) at rt for 30 min. The solution was concentrated in vacuo to remove TFA and the solvent. The residue was extracted with saturated solution of $NaHCO_3$ (20 mL) and CH_2Cl_2 (50 mL). The organic layer was collected, dehydrated with Na_2SO_4, and then concentrated. To the residue was added CH_2Cl_2 (50 mL), triethylamine (757 mg, 7.50 mmol), and chloroacetic anhydride (769 mg, 4.50 mmol). The solution was stirred for 4 h and washed with aqueous hydrochloric acid (1 M, 20 mL). The organic phase was dried with anhydrous Na_2SO_4 and then concentrated. The residue was purified with silica gel column chromatography using CH_2Cl_2/MeOH (20/1) as the eluent to

Scheme 2. Synthesis of SG-RB

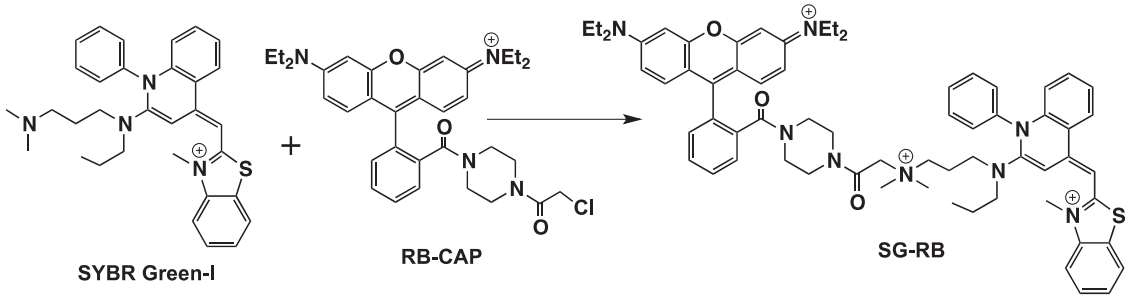

DOI: 10.1021/acs.analchem.9b04364
Anal. Chem. 2019, 91, 15899−15907

Scheme 3. Synthesis of SG-C_6-RB

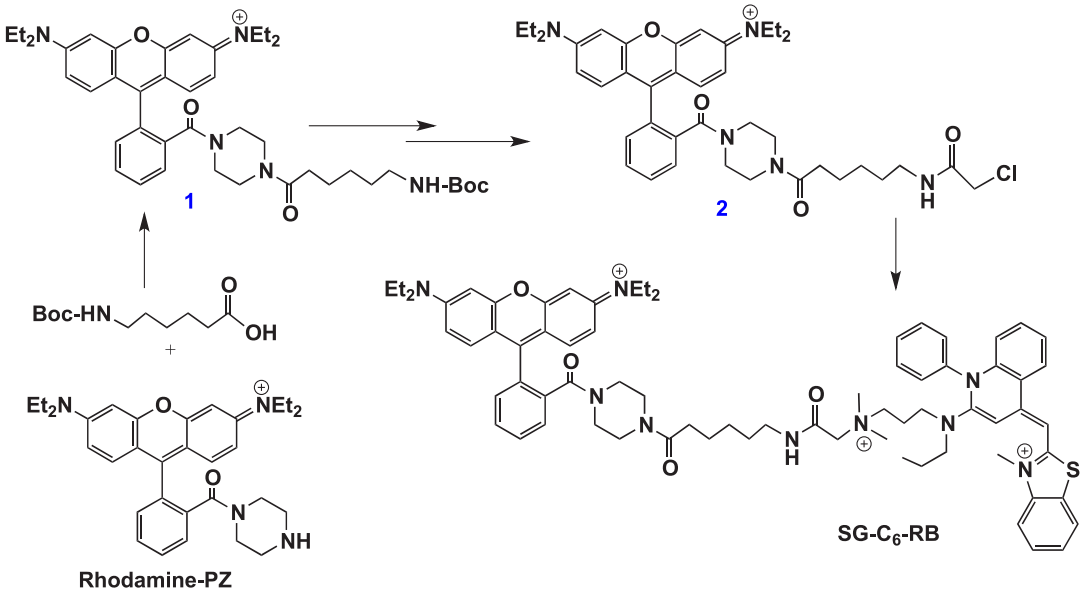

afford compound **2** (740 mg, 70%). ^{1}H NMR (500 MHz, DMSO-d_6) δ 8.36 (s, 1H), 7.80−7.68 (m, 3H), 7.55−7.51 (m, 1H), 7.19−7.08 (m, 4H), 6.95 (d, J = 2.1 Hz, 2H), 4.05 (dd, J = 5.5, 2.8 Hz, 2H), 3.66 (q, J = 7.1 Hz, 8H), 3.32−3.14 (m, 8H), 3.10−2.98 (m, 4H), 2.26 (t, J = 7.5 Hz, 2H), 1.43 (dt, J = 22.2, 7.4 Hz, 4H), 1.21 (dt, J = 7.3, 3.6 Hz, 12H). ^{13}C NMR (126 MHz, DMSO) δ 170.71, 165.71, 157.04, 155.56, 155.09, 135.24, 131.74, 130.69, 130.38, 129.73, 127.50, 114.30, 113.01, 95.90, 54.91, 45.40, 45.29, 42.68, 38.72, 28.63, 25.98, 24.29, 12.43, 8.49.

To a flask containing DMF (5 mL) were added SYBR Green-I (250 mg, 0.49 mmol), compound **2** (455 mg, 0.65 mmol), K_2CO_3 (209 mg, 1.51 mmol), and NaI (376 mg, 2.52 mmol). The mixture was stirred at 60 °C overnight and then concentrated in vacuo. The residue was subjected to silica gel column chromatography (CH_2Cl_2/MeOH = 10/1) to give SG-C_6-RB in 85% yield (490 mg). ^{1}H NMR (500 MHz, DMSO-d6) δ 9.43 (d, J = 20.9 Hz, 1H), 8.71 (dd, J = 8.6, 1.5 Hz, 1H), 8.29 (dd, J = 7.9, 1.2 Hz, 1H), 7.80−7.72 (m, 7H), 7.72−7.64 (m, 3H), 7.62−7.54 (m, 2H), 7.52 (dd, J = 5.8, 3.1 Hz, 1H), 7.39−7.33 (m, 1H), 7.17−7.07 (m, 5H), 7.05 (s, 1H), 6.93 (q, J = 2.0, 1.2 Hz, 2H), 6.85 (s, 1H), 4.32−4.25 (m, 2H), 4.01 (s, 3H), 3.64 (q, J = 7.3, 6.8 Hz, 8H), 3.51 (t, J = 8.2 Hz, 2H), 3.43 (d, J = 7.3 Hz, 2H), 3.20 (s, 14H), 3.12 (t, J = 7.7 Hz, 2H), 2.98 (s, 2H), 2.28−2.15 (m, 2H), 1.96 (q, J = 9.1, 7.5 Hz, 2H), 1.35 (s, 6H), 1.23 (d, J = 7.1 Hz, 2H), 1.18 (t, J = 7.0 Hz, 12H), 0.70 (t, J = 7.3 Hz, 3H). 13C NMR (126 MHz, DMSO) δ 170.68, 162.92, 162.84, 159.27, 157.65, 157.01, 155.54, 155.07, 148.99, 147.12, 140.68, 140.29, 138.60, 135.20, 132.55, 131.72, 130.59, 129.77, 129.55, 128.01, 125.18, 123.73, 123.43, 121.69, 112.99, 112.51, 106.43, 105.66, 102.31, 99.50, 95.88, 95.88, 62.07, 51.36, 48.70, 48.53, 45.41, 33.79, 33.78, 33.06, 32.17, 29.01, 28.31, 26.04, 24.20, 21.48, 20.50, 19.75, 12.44, 11.01, 7.50. MS (ES+) calcd for $C_{72}H_{88}N_9O_4S^{3+}$ (M^{3+}) m/z = 1174.6664/3 = 391.5555. Found: 391.5554.

Fluorescence Analysis on Probe Responses to Plasmid DNA. SG-RB or SG-C_6-RB (2 μM) was incubated in PBS (10.0 mM, pH 7.5) containing plasmid DNA (0, 0.18, 0.9, 1.8 mg/mL) for 0.5 h and then analyzed for fluorescence emission using an excitation wavelength of 490 nm.

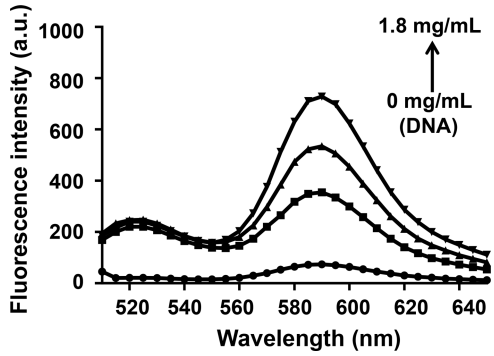

Figure 1. Fluorescence responses of SG-RB to plasmid DNA. SG-RB (2 μM) was incubated with PET22b (+) plasmid DNA (0, 0.18, 0.9, 1.8 mg/mL) for 0.5 h in phosphate buffered saline (PBS, 10.0 mM, pH 7.5) and then analyzed for fluorescence emission using an excitation wavelength of 490 nm.

Effects of DNAase on Fluorescence Emission of SG-RB/Plasmid DNA. SG-RB (9 μM) was incubated with plasmid DNA (0.16 mg/mL) for 4 h in PBS (10.0 mM, pH 7.4) and then spiked with DNAase to a final concentration of 0.16 mg/mL. The solution was maintained at 37 °C for 0, 0.5, 1, 1.5, 2, 17, or 19 h, and then the fluorescence emission was analyzed using an excitation wavelength of 490 nm.

Live Cell Imaging of mtDNA with SG-RB. HeLa cells were cultured in DMEM spiked with SG-RB (1 μM), LysoTracker Blue (1 μM), and MitoTracker Deep Red (0.5 μM) for 30 min. The cells were rinsed and then imaged by confocal fluorescence microscopy.

Dose-Dependent Staining of mtDNA with SG-RB. HeLa cells were cultured with 0.1, 0.2, 1.0, 2.0, or 5.0 μM SG-RB for 30 min and then visualized by confocal microscopy.

Potential-Dependent Staining of mtDNA with SG-RB. HeLa cells were cultured with SG-RB (1 μM) and Hoechst (5 μg/mL) in DMEM for 30 min and then cultivated with or without CCCP (50 μM) for 15 min. The cells were visualized by confocal microscopy.

Structure−Activity Relation (SAR) Analysis on mtDNA Imaging with SG-RB Analogues. HeLa cells were treated

DOI: 10.1021/acs.analchem.9b04364
Anal. Chem. 2019, 91, 15899−15907

with SG-RB (1 μM), SYBR-Green (1 μM), rhodamine-PZ (1 μM), or SG-C_6-RB (40 μM) for 30 min and then further cultured in DMEM containing Hoechst (5 μg/mL) and MitoTracker Deep Red (0.5 μM) in cell growth media for 30 min. The cells were rinsed with DMEM and then imaged by confocal fluorescence microscopy.

Retention of SG-RB with mtDNA. HeLa cells were incubated with SG-RB (1 μM) in DMEM for 30 min and then incubated in fresh DMEM for 0−72 h. The cells were washed with DMEM three times and then analyzed by confocal fluorescence microscopy for intracellular fluorescence at 0, 24, 48, and 72 h postincubation.

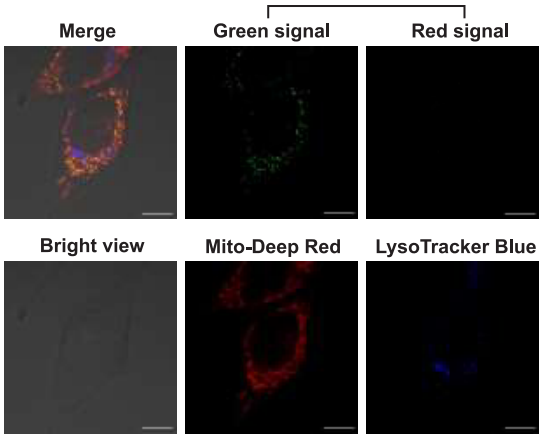

Figure 2. "Turn-on" fluorescence imaging of mtDNA with SG-RB. HeLa cells were cocultured with SG-RB (1.0 μM), LysoTracker Blue (1.0 μM), and Mito-Tracker Deep Red (0.5 μM) for 30 min. The cells were washed and then imaged by confocal fluorescence microscopy. Scale bars: 10 μm.

Cytotoxicity of SG-RB. HeLa cells were cultured in a 24-well cell culture plate containing SG-RB (0, 1, 2, 4, 8 μM) for 60 min and then maintained in DMEM for 0, 24, or 48 h. The cell number and cell viability were determined by MTT assay.

Effects of Mitophagy on Intracellular Fluorescence of SG-RB. *Basal Autophagy.* HeLa cells were cultured in DMEM spiked with SG-RB (1 μM), LysoTracker Blue (1 μM), and MitoTracker Deep Red (0.5 μM) for 30 min. The cells were washed with PBS three times and then incubated in fresh DMEM for 6 h before confocal microscopic analysis.

Elevated Autophagy. HeLa cells were first cultured in DMEM spiked with SG-RB (1 μM) for 30 min. The cells were washed with PBS three times and then incubated in DMEM supplemented with CCCP (50 μM) for 6 h before confocal microscopic analysis.

Inhibited Autophagy. HeLa cells were first cultured in DMEM spiked with SG-RB (1 μM) for 30 min. The cells were washed with PBS three times and then incubated in DMEM supplemented with Baf-A1 (60 nM) for 6 h before confocal microscopic analysis.

Effects of Doxorubicin on mtDNA. HeLa cells were first cultured in DMEM spiked with SG-RB (1 μM) for 30 min and then incubated with 0, 2, 5, or 10 μg of DOX for 24 h before confocal microscopy analysis.

RESULTS AND DISCUSSION

In Vitro Analysis on Binding of SG-RB to DNA. SG-RB was readily synthesized in 80% yield via one-step alkylation of SYBR Green-I with 1-(rhodamine B)-4-(2′-chloroacetyl)-piperazine amide (RB-CAP) (Scheme 2). We first tested the fluorescence response of SG-RB to purified PET22b (+) plasmid vector in vitro. SG-RB exhibited null green SG fluorescence in the absence of plasmid DNA, but robust green fluorescence peaked

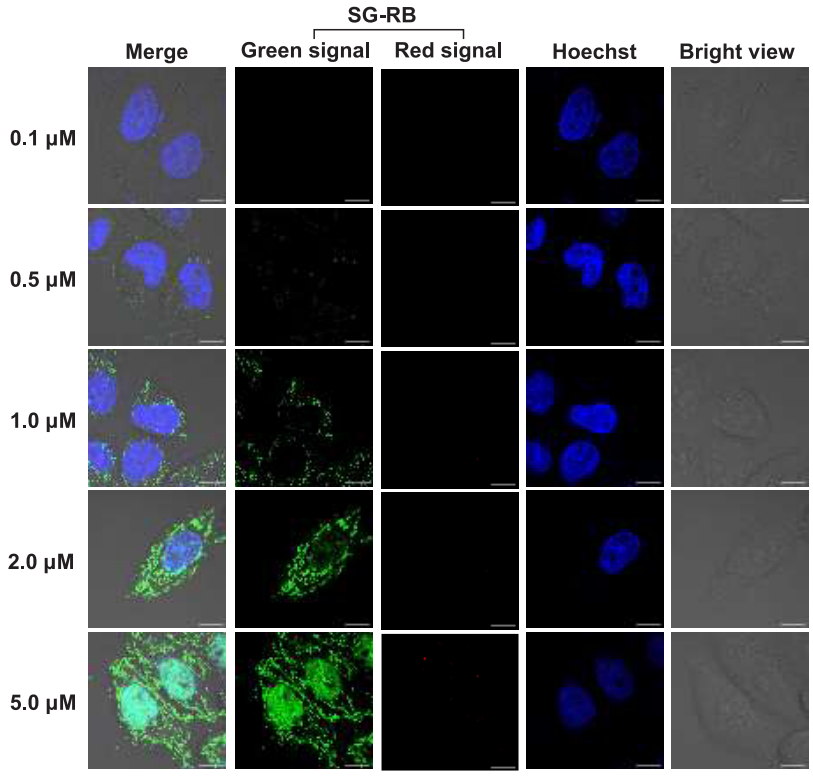

Figure 3. Preferred staining of mtDNA over nuDNA with SG-RB. HeLa cells were cultured with SG-RB (0.1, 0.5, 1.0, 2.0, or 5.0 μM) and Hoechst (1.0 μM) for 30 min and then imaged by confocal fluorescence microscopy. Scale bar: 10 μm.

DOI: 10.1021/acs.analchem.9b04364
Anal. Chem. 2019, 91, 15899−15907

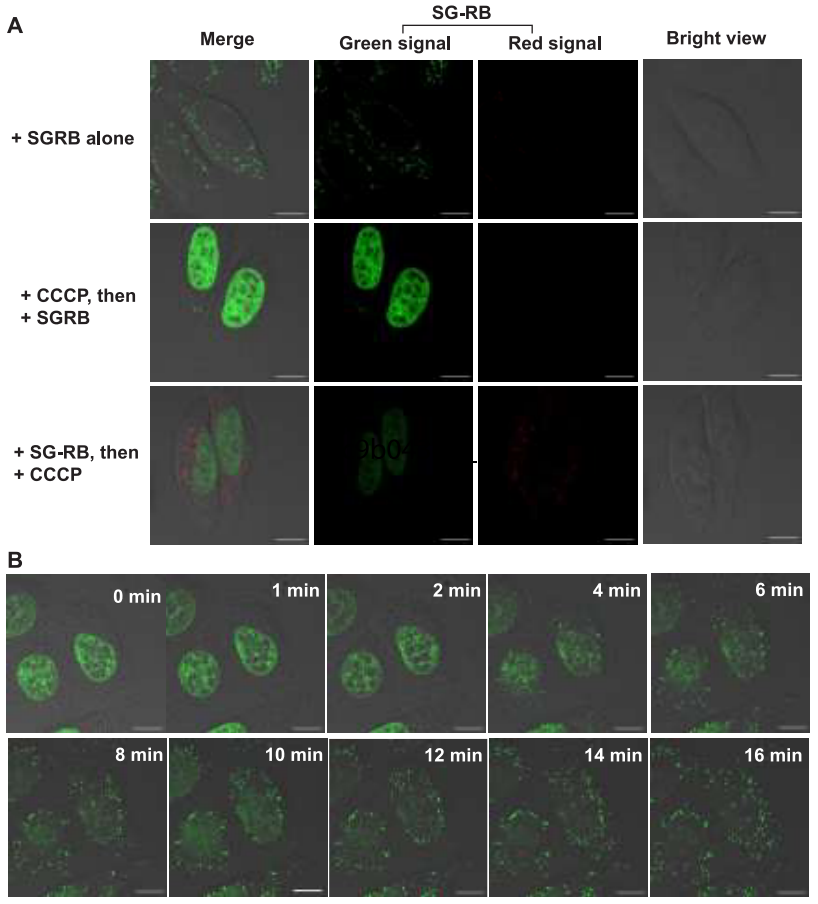

Figure 4. ΔΨm-mediated imaging of mtDNA over nuDNA with SG-RB. (A) HeLa cells were cultured with SG-RB (1.0 μM) for 30 min prior to or after 6 h of treatment with CCCP (50 μM) using cells loaded with SG-RB alone as the control. The cells were visualized by confocal microscopy for intracellular fluorescence. (B) Relocation of SG-RB from nuDNA into mtDNA upon ΔΨm recovery. HeLa cells were treated with SG-RB (1.0 μM) for 30 min and then for 15 min with CCCP (50.0 μM). The cells were maintained in fresh DMEM for 0−16 min and then imaged by confocal microscopy at indicated time points. Scale bars: 10 μm.

at 525 nm after incubation with plasmid DNA (Figure 1), showing fluorogenic binding of SG domain to DNA as proposed in Scheme 1. To further confirm DNA-mediated SG fluorescence, we examined the effects of DNAase on DNA/SG-RB complex and observed SG fluorescence fading off over time in the presence of DNAase (Figure S1). In contrast to the relatively constant SG fluorescence triggered by DNA plasmid, SG-RB displayed dose-correlated rhodamine fluorescence that is centered at 590 nm (Figure 1). Historically, rhodamine-labeled proteins, with self-quenched fluorescence of pendant rhodamines, have been reported for fluorescence-on imaging of proteases.[28] Similarly, the attenuated rhodamine fluorescence of SG-RB at lower levels of DNA (0.18 vs 1.8 mg/mL) suggests greater fluorescence quenching due to more densely populated rhodamines of closer proximity on DNA. Collectively, these results show DNA binding-mediated "on−off" green fluorescence of SG-RB, which is beneficial for low-background mtDNA imaging in live cells.

Live Cell Imaging of mtDNA with "Turn-On" Green SG Fluorescence of SG-RB in Mitochondria. With plasmid DNA-triggered green fluorescence, we were keen to determine whether SG-RB could target mtDNA in live cells. HeLa cells were costained with SG-RB, Lyso-Tracker Blue, and Mito-Tracker Deep Red, a dye specific for mitochondria. Confocal microscopic analysis revealed points of green fluorescence colocalized with Mito-Tracker Deep Red but not Lyso-Tracker Blue, an indicator of acidic lysosomes (Figure 2). Given DNA-specific SG fluorescence, these results showed that SG-RB selectively binds mtDNA in mitochondria, thereby giving rise to turn-on green fluorescence. To optimize the assay, HeLa cells were stained with varied concentrations of SG-RB and Hoechst indicative of nuDNA. Green fluorescence was identified exclusively in mitochondria in the presence of 0.1−2.0 μM of SG-RB, whereas nuDNA-associated green fluorescence emerged in cells treated with 5 μM of SG-RB (Figure 3). This showed that, after reaching full capacity of mtDNA, excess SG-RB would stain nuDNA. The applicability of SG-RB to image mtDNA was further validated in diverse cell lines including A-549, MCF-7, B16−F10, and Huh-7 (Figure S2), where mtDNA-specific green fluorescence remained detectable for at least 48 h (Figure S3). In addition, no detectable cytotoxicity was identified in cells loaded with SG-RB at doses up to 8 μM (Figure S4), which is beneficial for live cell mtDNA imaging.

ΔΨm-Mediated Selective Imaging of mtDNA over nuDNA via Turn-On Green Fluorescence of SG-RB. We then assessed the impact of ΔΨm on mtDNA imaging using cells pretreated with carbonyl cyanide *m*-chlorophenylhydrazone (CCCP), a protonophore capable of decreasing ΔΨm.[29] In contrast with selective targeting of mtDNA in control cells, SG-RB exclusively stained nuDNA in ΔΨm-suppressed $CCCP^+$ HeLa cells (Figure 4A), showing ΔΨm-dependent mtDNA staining by SG-RB. Partitioning of SG-RB in mitochondria

DOI: 10.1021/acs.analchem.9b04364
Anal. Chem. 2019, 91, 15899−15907

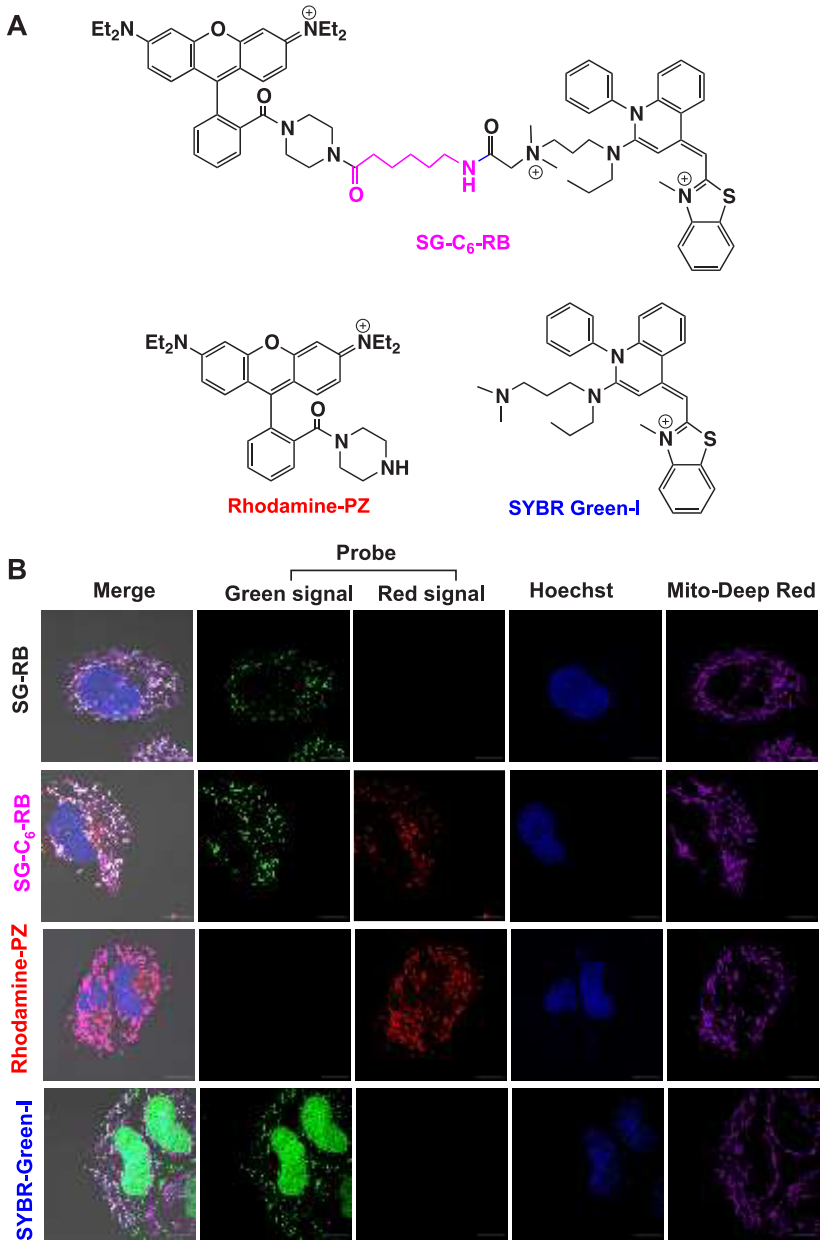

Figure 5. Cell imaging with structural analogues of SG-RB. (A) Chemical structure of SG-C_6-RB, rhodamine-PZ, and SYBR Green-I. (B) Distinct subcellular distribution of structural analogues of SG-RB. HeLa cells were treated with SG-RB (1 μM), SYBR Green-I (1.0 μM), rhodamine-PZ (1.0 μM), or SG-C_6-RB (40.0 μM) and then cocultured with Hoechst (5.0 μg/mL) and Mito-Tracker Deep Red (0.5 μM) for 30 min before confocal microscopy analysis. Scale bar: 10 μm.

driven by $\Delta\Psi$m leads to selective fluorescence labeling of mtDNA over nuDNA, whereas in CCCP-pretreated cells, SG-RB no longer accumulates in mitochondria and thus binds nuDNA owing to the intrinsic affinity of the SG moiety to nuDNA. Next, we explored the effects of $\Delta\Psi$m decrease on SG-RB preanchored in mtDNA. HeLa cells were stained with SG-RB and then cultured with CCCP. We observed significant relocation of SG-RB from mitochondria into nucleus induced by CCCP (Figures 4A and S5). Finally, we examined the effects of restored $\Delta\Psi$m on SG-RB preanchored in nuDNA. $CCCP^+$ HeLa were incubated with SG-RB to stain nuDNA and then maintained in fresh cell culture medium for varied periods of time to re-establish functional $\Delta\Psi$m. Time-lapse microscopy analysis revealed the rise of SG fluorescence in mitochondria over time with concomitant attenuation of SG fluorescence in nucleus (Figure 4B), showing probe migration from nuDNA into mtDNA upon restored $\Delta\Psi$m. Combined, these results show that the dynamic partitioning of SG-RB between mtDNA and nuDNA is critically controlled by $\Delta\Psi$m status in live cells.

SARs on Mitochondria-Directed mtDNA Imaging Using Structural Analogues of SG-RB. We noticed the lack of rhodamine fluorescence on binding of SG-RB to mtDNA or to nuNA inside cells (Figures 2 and 3). This is unexpected as SG-RB/plasmid DNA exhibited bright rhodamine fluorescence in vitro (Figure 1). To gain insight on this, SG-C_6-RB was synthesized as the structural analogue of SG-RB with an elongated spacer (Scheme 3), which exhibited a similar fluorescence property as SG-RB (Figures 5A and S6). SG-C_6-RB^+ cells exhibited both intense rhodamine fluorescence and SG fluorescence in mitochondria (Figure 5B), showing retention of rhodamine

DOI: 10.1021/acs.analchem.9b04364
Anal. Chem. 2019, 91, 15899−15907

fluorescence upon binding of SG-C_6-RB to mtDNA. The distinct linker effects demonstrated by fluorescence emission of SG-C_6-RB/mtDNA over SG-RB/mtDNA suggest that rhodamine fluorescence is quenched in SG-RB/mtDNA, which is likely due to physical contact of SG-RB with complex nucleoids that contain diverse proteins. Next, HeLa cells were stained with rhodamine-PZ or SYBR Green-I (Figure 5A), the equivalent of RB domain and SG domain of SG-RB, respectively. Rhodamine-PZ selectively stained mitochondria while SYBR Green-I is predominantly located in the nucleus (Figure 5B). Combined, these findings validate cationic RB moiety-conferred selectivity of SG-RB for mtDNA over nuDNA in live cells.

Correlation of Mitophagy with Turn-On Rhodamine Fluorescence of SG-RB in Lysosomes. Autophagy is an evolutionary conserved process by which organelles could be sequestered into autophagosomes which in turn fuse with acidic lysosomes to execute degradation.[30] Autophagic removal of excess or impaired mitochondria, known as mitophagy, is critical for mitochondria health, and defects in mitophagy have been linked to several diseases.[30] We observed rhodamine signals in cells subjected to a treatment process by SG-RB followed by CCCP; however, such signals were absent when the latter CCCP treatment was done first (Figure 4A). As $\Delta\Psi$m attenuation promotes autophagy, we thus explored the relevance of autophagy to rhodamine fluorescence. HeLa cells were loaded with SG-RB to stain mtDNA and then cultured in DMEM for varied periods of time. Absent at the initial stage of culturing (Figure 2), rhodamine signals occurred after 6 h culturing (Figure 6). In addition, the rhodamine signals are confined in

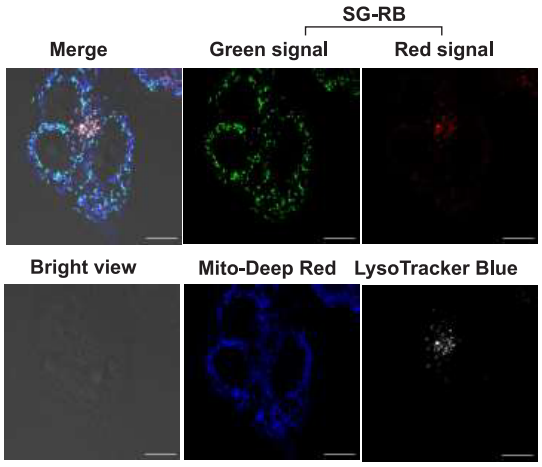

Figure 6. Extended incubation leading to formation of rhodamine fluorescence in lysosomes in SG-RB-loaded cells. SG-RB fluorescence in cells prestained with SG-RB. HeLa cells were cocultured with SG-RB (1 μM), LysoTracker Blue (1 μM), and Mito-Tracker Deep Red (0.5 μM) for 30 min. The cells were washed and then maintained in fresh culture medium for 0 or 6 h and then imaged by confocal fluorescence microscopy. Scale bars: 10 μm.

lysosomes where no green SG fluorescence could be identified (Figure S7). We anticipate that the lysosome-associated rhodamine fluorescence originates from basal mitophagy, by which delivery of mtDNA/SG-RB into lysosomes leads to release of SG-RB and thus restores rhodamine fluorescence (Figure 7A). To support this hypothesis, we tracked SG-RB/mtDNA in cells devoid of mitophagy using HeLa cells cultured with Bafilomycin A1 (Baf-A1). Baf-A1 is an inhibitor of proton vacuolar ATPase pump[31] and could block mitophagy influx by inhibiting fusion of

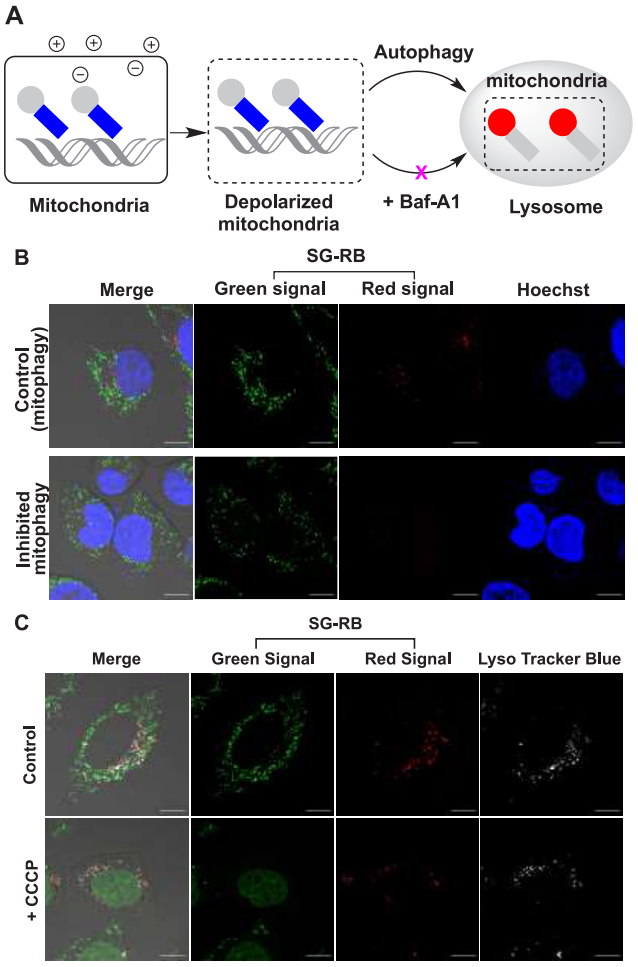

Figure 7. Mitophagy correlated rhodamine fluorescence of SG-RB. (A) Schematic for mitophagy-mediated delivery of SG-RB/mtDNA into lysosomes to switch green to red fluorescence. (B) Correlation of autophagy to rhodamine fluorescence of SG-RB. HeLa cells were maintained in DMEM spiked with SG-RB (1 μM) and Hoechst (5.0 μg/mL) for 30 min and then cultured for 6 h in DMEM supplemented with or without Baf-A1 (60 nM) before confocal microscopy analysis. (C) Lysosome-specific rhodamine fluorescence. HeLa cells were maintained in DMEM spiked with SG-RB (1.0 μM) and LysoTracker Blue (1.0 μM) for 30 min and then cultured for 6 h with or without CCCP (50.0 μM). These cells were visualized by confocal fluorescence microscopy. Scale bar: 10 μm.

autophagosomes with lysosomes.[32] Baf-A1$^+$ HeLa cells exhibited completely suppressed rhodamine signals (Figure 7B), thus supporting mitophagy-mediated rhodamine fluorescence in lysosomes. Finally, we determined the subcellular distribution of rhodamine signals in cells treated with a $\Delta\Psi$m suppressor (CCCP) (Figure 7C). HeLa cells prestained with SG-RB were treated with CCCP in combination with hoechst or LysoTracker Blue. Apart from nuDNA-associated SG fluorescence indicative of probe relocation from depolarized mitochondria into nucleus (Figure S7), bright rhodamine fluorescence was identified in lysosomes in CCCP$^+$ cells (Figure 7C), which supports delivery of SG-RB/mtDNA into lysosomes. Taken together, these findings suggest the use of SG-RB to discern mtDNA in mitophagy via turn-on red fluorescence in lysosomes from mtDNA in normal cells via green SG fluorescence in mitochondria.

Imaging mtDNA in Doxorubicin-Stressed Cells with SG-RB. With the dual-color imaging, SG-RB was evaluated for its performance to visualize mtDNA in HeLa cells stressed with

DOI: 10.1021/acs.analchem.9b04364
Anal. Chem. 2019, 91, 15899−15907

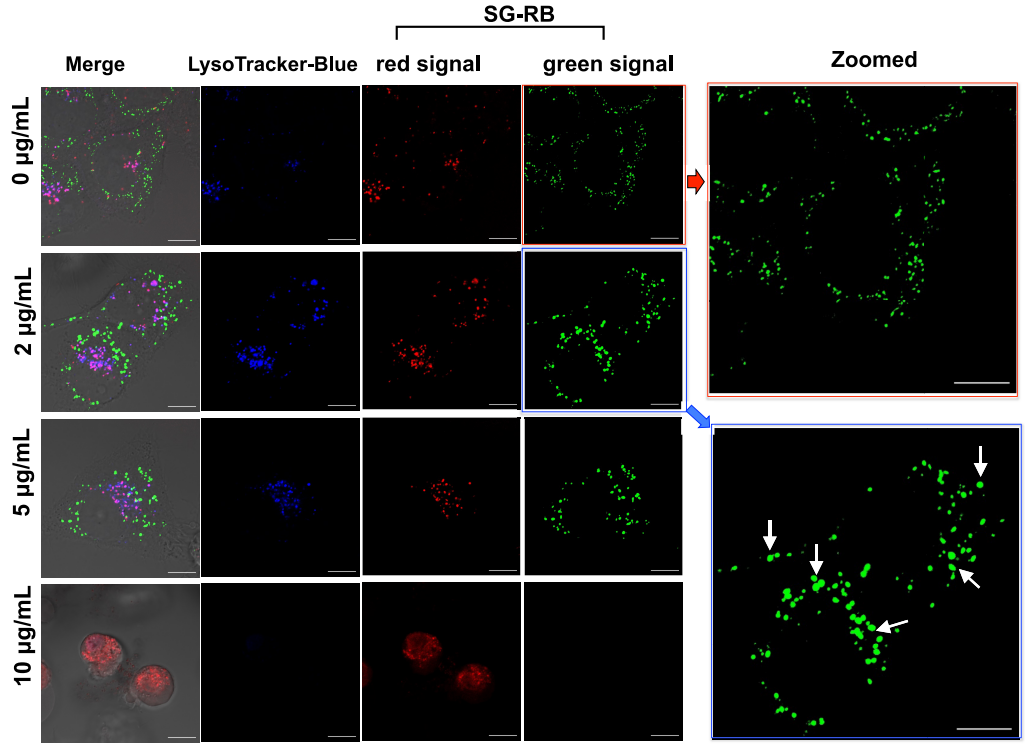

Figure 8. Doxorubicin induces mtDNA aggregation and promotes mitophagy. HeLa cells were first stained with SG-RB (1 μM) for 30 min and then incubated with 0, 2, 5, or 10 μg of Dox for 24 h before confocal microscopy analysis. Scale bars: 10 μm.

Doxorubicin (Dox), a potent anticancer drug shown to damage mitochondrial DNA and induce mitochondrial dysfunctions.[33−37] After 24 h of incubation with Dox, cells formed enlarged points of SG fluorescence in mitochondria elicited by Dox (2−5 μg/mL), showing mtDNA aggregation induced by Dox. Moreover, 10 μg/mL of Dox caused massive rhodamine signals and the loss of SG fluorescence (Figure 8), indicative of Dox-promoted mitophagy. These observations are consistent with recently reported effects of Dox to induce mitophagy,[38−40] demonstrating the feasibility of SG-RB to image mtDNA responses to chemotherapeutics. To date, distinct strategies have been designed for tracking delivery of mitochondria into acidic lysosomes in autophagy[41−48] or sensing of $\Delta\Psi$m changes,[49−51] two processes often interwined in cell stress. Complementing these approaches, our method focuses on analyzing mtDNA in normal cells and autophagy, a transition relevant to the pathological roles of mtDNA, using a chameleon probe prone to $\Delta\Psi$m-mediated partitioning in mitochondria.

CONCLUSIONS

Mitochondrial DNA plays important roles in diverse physiological processes as well as myriad pathological events such as inflammation and inherited diseases. We herein demonstrated dual-color imaging of mtDNA with SG-RB, an organelle-trappable DNA sensor, which integrates a SYBR Green-I entity for fluorogenic DNA sensing and a cationic rhodamine entity for targeting of mitochondria. SG-RB selectively stains mtDNA over nuDNA, thereby giving turn-on green SG fluorescence. Upon mitophagic delivery of SG-RB/mtDNA into lysosomes, SG-RB exhibits restored red fluorescence together with the loss of green fluorescence. Aided with the distinct color switch of SG-RB/mtDNA in mitochondria over lysosomes, marked mtDNA aggregation and elevated mitophagy were uncovered in cells stressed with the anticancer drug Doxorubicin. Live cell imaging of mtDNA with classical DNA sensors is challenging owing to interference of nuDNA. Complementing de novo design of mtDNA-reporting agents[12−15] and intraorganelle bioorthogonal chemistries,[52−55] our method takes advantage of organelle-directed fluorogenic intercalation to achieve live cell imaging of mtDNA, which would facilitate the study of dynamic mtDNA, a major danger-associated molecular pattern underlying diverse pathological disorders.

ASSOCIATED CONTENT

Supporting Information

The Supporting Information is available free of charge at https://pubs.acs.org/doi/10.1021/acs.analchem.9b04364.

Analysis spectra of SG-RB and SG-C_6-RB, cell imaging of mtDNA with SG-RB in different cells lines, and temporal retention and cytotoxicity of SG-RB (PDF)

AUTHOR INFORMATION

Corresponding Author

*E-mail: shoufa@xmu.edu.cn.

ORCID

Shoufa Han: 0000-0002-2057-0559

Author Contributions

§X.Z. and Y.S. contributed equally to this work.

Notes

The authors declare no competing financial interest.

ACKNOWLEDGMENTS

This work was supported by grants from NSF China (21775130, 91854106, 81788101, and 21572189). We thank Boyu Han at University of California Riverside for assistance in English composition, and associated Professor Liu Yang for helpful discussion.

DOI: 10.1021/acs.analchem.9b04364
Anal. Chem. 2019, 91, 15899−15907

REFERENCES

(1) Friedman, J. R.; Nunnari, J. *Nature* **2014**, *505*, 335−343.
(2) Green, D. R. *Cell* **1998**, *94*, 695−698.
(3) Lin, M. T.; Beal, M. F. *Nature* **2006**, *443*, 787−795.
(4) Taanman, J. W. *Biochim. Biophys. Acta, Bioenerg.* **1999**, *1410*, 103−123.
(5) Gray, M. W. *Annu. Rev. Cell Biol.* **1989**, *5*, 25−50.
(6) Baudouin, S. V.; Saunders, D.; Tiangyou, W.; Elson, J. L.; Poynter, J.; Pyle, A.; Keers, S.; Turnbull, D. M.; Howell, N.; Chinnery, P. F. *Lancet* **2005**, *366*, 2118−2121.
(7) Shimada, K.; Crother, T. R.; Karlin, J.; Dagvadorj, J.; Chiba, N.; Chen, S.; Ramanujan, V. K.; Wolf, A. J.; Vergnes, L.; Ojcius, D. M.; Rentsendorj, A.; Vargas, M.; Guerrero, C.; Wang, Y.; Fitzgerald, K. A.; Underhill, D. M.; Town, T.; Arditi, M. *Immunity* **2012**, *36*, 401−414.
(8) West, A. P.; Shadel, G. S. *Nat. Rev. Immunol.* **2017**, *17*, 363−375.
(9) Latorre-Pellicer, A.; Moreno-Loshuertos, R.; Lechuga-Vieco, A. V.; Sanchez-Cabo, F.; Torroja, C.; Acin-Perez, R.; Calvo, E.; Aix, E.; Gonzalez-Guerra, A.; Logan, A.; Bernad-Miana, M. L.; Romanos, E.; Cruz, R.; Cogliati, S.; Sobrino, B.; Carracedo, A.; Perez-Martos, A.; Fernandez-Silva, P.; Ruiz-Cabello, J.; Murphy, M. P.; Flores, I.; Vazquez, J.; Enriquez, J. A. *Nature* **2016**, *535*, 561−565.
(10) Oka, T.; Hikoso, S.; Yamaguchi, O.; Taneike, M.; Takeda, T.; Tamai, T.; Oyabu, J.; Murakawa, T.; Nakayama, H.; Nishida, K.; Akira, S.; Yamamoto, A.; Komuro, I.; Otsu, K. *Nature* **2012**, *485*, 251−255.
(11) Yousefi, S.; Mihalache, C.; Kozlowski, E.; Schmid, I.; Simon, H. U. *Cell Death Differ.* **2009**, *16*, 1438−1444.
(12) Lentz, S. I.; Edwards, J. L.; Backus, C.; McLean, L. L.; Haines, K. M.; Feldman, E. L. *J. Histochem. Cytochem.* **2010**, *58*, 207−218.
(13) Ligasova, A.; Strunin, D.; Koberna, K. *PLoS One* **2013**, *8*, No. e66864.
(14) Shen, Y.; Shao, T.; Fang, B.; Du, W.; Zhang, M.; Liu, J.; Liu, T.; Tian, X.; Zhang, Q.; Wang, A.; Yang, J.; Wu, J.; Tian, Y. *Chem. Commun.* **2018**, *54*, 11288−11291.
(15) Gao, F.; Li, L.; Fan, J.; Cao, J.; Li, Y.; Chen, L.; Peng, X. *Anal. Chem.* **2019**, *91*, 3336−3341.
(16) Briggs, C.; Jones, M. *Acta Histochem.* **2005**, *107*, 301−312.
(17) Chazotte, B. *Cold Spring Harb. Protoc.* **2012**, *2012*, 892−894.
(18) Asin-Cayuela, J.; Manas, A. R.; James, A. M.; Smith, R. A.; Murphy, M. P. *FEBS Lett.* **2004**, *571*, 9−16.
(19) Yuan, H.; Cho, H.; Chen, H. H.; Panagia, M.; Sosnovik, D. E.; Josephson, L. *Chem. Commun.* **2013**, *49*, 10361−10363.
(20) Abu-Gosh, S. E.; Kolvazon, N.; Tirosh, B.; Ringel, I.; Yavin, E. *Mol. Pharmaceutics* **2009**, *6*, 1138−1144.
(21) Wang, H.; Chang, J.; Shi, M.; Pan, W.; Li, N.; Tang, B. *Angew. Chem., Int. Ed.* **2019**, *58*, 1057−1061.
(22) Velusamy, N.; Binoy, A.; Bobba, K. N.; Nedungadi, D.; Mishra, N.; Bhuniya, S. *Chem. Commun.* **2017**, *53*, 8802−8805.
(23) Xu, W.; Zeng, Z.; Jiang, J. H.; Chang, Y. T.; Yuan, L. *Angew. Chem., Int. Ed.* **2016**, *55*, 13658−13699.
(24) Ma, C.; Wei, C.; Li, X.; Zheng, X.; Chen, B.; Wang, M.; Zhang, P.; Li, X. *Dyes Pigm.* **2019**, *162*, 624−631.
(25) Chen, X.; Wu, S.; Han, J.; Han, S. *Bioorg. Med. Chem. Lett.* **2013**, *23*, 5295−5299.
(26) Konnai, S.; Usui, T.; Ohashi, K.; Onuma, M. *Vet. Microbiol.* **2003**, *94*, 283−294.
(27) Ricketts, H. J.; Morgan, A. J.; Spurgeon, D. J.; Kille, P. *Ecotoxicol. Environ. Saf.* **2004**, *57*, 4−10.
(28) Weissleder, R.; Tung, C. H.; Mahmood, U.; Bogdanov, A., Jr. *Nat. Biotechnol.* **1999**, *17*, 375−378.
(29) Heytler, P. G. *Biochemistry* **1963**, *2*, 357−361.
(30) Mizushima, N. *Genes Dev.* **2007**, *21*, 2861−2873.
(31) Yoshimori, T.; Yamamoto, A.; Moriyama, Y.; Futai, M.; Tashiro, Y. *J. Biol. Chem.* **1991**, *266*, 17707−17712.
(32) Mauvezin, C.; Neufeld, T. P. *Autophagy* **2015**, *11*, 1437−1438.
(33) Nitiss, K. C.; Nitiss, J. L. *Clin. Cancer Res.* **2014**, *20*, 4737−4739.
(34) Gorini, S.; De Angelis, A.; Berrino, L.; Malara, N.; Rosano, G.; Ferraro, E. *Oxid. Med. Cell. Longevity* **2018**, *2018*, 7582730.
(35) Zhou, S.; Starkov, A.; Froberg, M. K.; Leino, R. L.; Wallace, K. B. *Cancer Res.* **2001**, *61*, 771−777.
(36) Montaigne, D.; Marechal, X.; Preau, S.; Baccouch, R.; Modine, T.; Fayad, G.; Lancel, S.; Neviere, R. *Mitochondrion* **2011**, *11*, 22−26.
(37) Green, P. S.; Leeuwenburgh, C. *Biochim. Biophys. Acta, Mol. Basis Dis.* **2002**, *1588*, 94−101.
(38) Koleini, N.; Kardami, E. *Oncotarget* **2017**, *8*, 46663−46680.
(39) Catanzaro, M. P.; Weiner, A.; Kaminaris, A.; Li, C.; Cai, F.; Zhao, F.; Kobayashi, S.; Kobayashi, T.; Huang, Y.; Sesaki, H.; Liang, Q. *FASEB J.* **2019**, *33*, 11096.
(40) Yin, J.; Guo, J.; Zhang, Q.; Cui, L.; Zhang, L.; Zhang, T.; Zhao, J.; Li, J.; Middleton, A.; Carmichael, P. L.; Peng, S. *Toxicol. In Vitro* **2018**, *51*, 1−10.
(41) Lee, M. H.; Park, N.; Yi, C.; Han, J. H.; Hong, J. H.; Kim, K. P.; Kang, D. H.; Sessler, J. L.; Kang, C.; Kim, J. S. *J. Am. Chem. Soc.* **2014**, *136*, 14136−14142.
(42) Katayama, H.; Kogure, T.; Mizushima, N.; Yoshimori, T.; Miyawaki, A. *Chem. Biol.* **2011**, *18*, 1042−1052.
(43) Hu, F.; Cai, X.; Manghnani, P. N.; Kenry; Wu, W.; Liu, B. *Chem. Sci.* **2018**, *9*, 2756−2761.
(44) Zou, Z.; Yan, Q.; Ai, S.; Qi, P.; Yang, H.; Zhang, Y.; Qing, Z.; Zhang, L.; Feng, F.; Yang, R. *Anal. Chem.* **2019**, *91*, 8574−8581.
(45) Niu, L. Q.; Huang, J.; Yan, Z. J.; Men, Y. H.; Luo, Y.; Zhou, X. M.; Wang, J. M.; Wang, J. H. *Spectrochim. Acta, Part A* **2019**, *207*, 123−131.
(46) Iwashita, H.; Torii, S.; Nagahora, N.; Ishiyama, M.; Shioji, K.; Sasamoto, K.; Shimizu, S.; Okuma, K. *ACS Chem. Biol.* **2017**, *12*, 2546−2551.
(47) Leung, C. W.; Wang, Z.; Zhao, E.; Hong, Y.; Chen, S.; Kwok, R. T.; Leung, A. C.; Wen, R.; Li, B.; Lam, J. W.; Tang, B. Z. *Adv. Healthcare Mater.* **2016**, *5*, 427−431.
(48) Li, X.; Hu, Y.; Li, X.; Ma, H. *Anal. Chem.* **2019**, *91*, 11409−11416.
(49) Xue, Z.; Zhao, H.; Liu, J.; Han, J.; Han, S. *Chem. Sci.* **2017**, *8*, 1915−1921.
(50) Xue, Z.; Zhao, H.; Liu, J.; Han, J.; Han, S. *Anal. Chem.* **2017**, *89*, 7795−7801.
(51) Tian, M.; Sun, J.; Dong, B.; Lin, W. *Angew. Chem., Int. Ed.* **2018**, *57*, 16506−16510.
(52) Xue, Z.; Zhang, E.; Liu, J.; Han, J.; Han, S. *Angew. Chem., Int. Ed.* **2018**, *57*, 10096−10101.
(53) Xue, Z.; Zhu, R.; Wang, S.; Li, J.; Han, J.; Liu, J.; Han, S. *Anal. Chem.* **2018**, *90*, 2954−2964.
(54) Logan, A.; Pell, V. R.; Shaffer, K. J.; Evans, C.; Stanley, N. J.; Robb, E. L.; Prime, T. A.; Chouchani, E. T.; Cocheme, H. M.; Fearnley, I. M.; Vidoni, S.; James, A. M.; Porteous, C. M.; Partridge, L.; Krieg, T.; Smith, R. A.; Murphy, M. P. *Cell Metab.* **2016**, *23*, 379−385.
(55) Tomas-Gamasa, M.; Martinez-Calvo, M.; Couceiro, J. R.; Mascarenas, J. L. *Nat. Commun.* **2016**, *7*, 12538.
(56) Wu, S.; Song, Y.; Li, Z.; Wu, Z.; Han, J.; Han, S. *Anal. Methods* **2012**, *4*, 1699−1703.
(57) Garger, S. J.; Griffith, O. M.; Grill, L. K. *Biochem. Biophys. Res. Commun.* **1983**, *117*, 835−842.

DOI: 10.1021/acs.analchem.9b04364
Anal. Chem. 2019, 91, 15899−15907